Catalysis Today 225 (2014) 96–101

Contents lists available at ScienceDirect

Catalysis Today

journal homepage: www.elsevier.com/locate/cattod

A dopant-mediated recombination mechanism in Fe-doped TiO_2 nanoparticles for the photocatalytic decomposition of nitric oxide

Qingping Wu[a], Chieh-Chao Yang[b], Roel van de Krol[a,*]

[a] Materials for Energy Conversion and Storage, Department of Chemical Engineering, Delft University of Technology, P.O. Box 5045, 2600 GA Delft, The Netherlands

[b] Photocatalytic Synthesis Laboratory, Faculty of Science and Technology, University of Twente, P.O. Box 217, 7500 AE Enschede, The Netherlands

ARTICLE INFO

Article history:
Received 2 July 2013
Received in revised form
11 September 2013
Accepted 18 September 2013
Available online 13 October 2013

Keywords:
Photocatalysis
TiO_2
Nanoparticles
Fe-doping
Nitric oxide
IR spectroscopy

ABSTRACT

The photon-assisted adsorption and catalytic decomposition of nitric oxide (NO) over undoped and Fe-doped TiO_2 nanoparticles have been investigated by in situ diffuse reflectance infrared Fourier transformed (DRIFT) spectroscopy, in situ X-ray photoelectron spectroscopy (XPS) and on-line NO_x analysis. The DRIFT spectra and on-line NO_x analysis reveal that the usual photo-oxidation of NO to NO_2 is strongly suppressed by the Fe dopant. This is found to be caused by the photo-reduction of Fe^{3+} to Fe^{2+}, which is an effective adsorption site for nitric oxide species. The DRIFT spectra indeed reveal a new band at 1805 cm^{-1}, which is assigned to the N=O stretch vibration in a $Fe^{2+}(NO)_2$ complex. Instead of producing NO_2, photo-generated hydroxyl radicals oxidize the Fe^{2+} back to Fe^{3+}. This causes the NO to desorb again, effectively closing an NO-mediated recombination loop. These results support the recently proposed reaction mechanisms for the photocatalytic decomposition of NO over undoped and Fe-doped TiO_2, and provide new insights for the development of highly selective photocatalysts based on doped metal oxides.

1. Introduction

NO_x is one of the most harmful environmental pollutants in air. It causes damage to the lung tissue of human beings, and contributes to the formation of acid rain and depletion of the ozone layer [1]. The emission of NO_x, a mixture of NO and NO_2 [2], is mainly produced by the chemical reaction of N_2 and O_2 during the high-temperature combustion of fossil fuels in air [3,4]. Although NO_x emissions have slightly decreased since the late 1990s, concerns are that they will greatly increase again due to the growing number of automobiles in developing countries. Many technologies have been devoted to the removal of NO_x, including NO_x storage and reduction catalysis (NSR), selective catalytic reduction (SCR) and photocatalysis [5,2]. The photocatalysis route is arguably the most attractive one, since it can remove NO_x in dilute form from air at room temperature. TiO_2, one of the most popular photocatalysts, is particularly efficient at decomposing NO_x [6].

The photocatalytic activity of TiO_2 originates from the presence of photo-generated electrons (e^-) in the conduction band and holes (h^+) in the valence band under irradiation with UV light [7]. However, these excited electrons and holes are not stable and can quickly recombine, releasing their energy in the form of heat [8]. To ensure that a sufficiently large fraction of the carriers can reach the surface before recombining, TiO_2 is generally studied in nanostructured form. Once the electrons and holes arrive at the surface, they react with adsorbed oxygen to form superoxide anions and hydroxyl radicals, respectively [9,10]. These species further react with adsorbed NO_x to form surface nitrates [11,12]. These nitrates do not spontaneously desorb and thus de-activate the catalyst until they are washed away by rain. To avoid this de-activation, several efforts have been made to change the selectivity of the photocatalytic reaction so that NO_x is photo-reduced to N_2 and O_2, both of which easily desorb from the surface. Anpo et al. showed that highly dispersed tetrahedrally-coordinated 'TiO_2' clusters in zeolites can indeed photo-reduce NO_x into N_2 and O_2 [13]. The reaction mechanism, however, remains unclear [14]. More recently, we have reported an alternative, more economical NO photoreduction catalyst in the form of nanostructured Fe-doped TiO_2 [15]. We elucidated the adsorption of NO species at the Fe/TiO_2 surface [16], and proposed a mechanism that explains how the photo-reduction of the Fe^{3+} dopant changes the selectivity of the NO decomposition reaction [15]. In this paper, we will show direct experimental evidence that further supports this reaction mechanism.

* Corresponding author. Present address: Helmholtz-Zentrum Berlin für Materialien und Energie Gmbh, Institute for Solar Fuels, Hahn-Meitner-Platz 1, 14109 Berlin, Germany. Tel.: +49 30 806243035.
E-mail address: roel.vandekrol@helmholtz-berlin.de (R. van de Krol).

0920-5861/$ – see front matter © 2013 Elsevier B.V. All rights reserved.
http://dx.doi.org/10.1016/j.cattod.2013.09.026

2. Methods and materials

2.1. Photocatalyst preparation

Undoped (pure) titanium dioxide (TiO_2) and 1% Fe-doped TiO_2 nanoparticles were synthesized by a simple, template-free sol–gel method [16]. For preparing 1% Fe/TiO_2, 0.8311 g of $Fe(NO_3)_3 \cdot 9H_2O$ (+99%, Acros) was fully dissolved in 375 ml ultrapure water (Milli-Q, 18.2 MΩ cm) and mixed with 2.6 ml HNO_3 (65% in H_2O) resulting in the formation of clear yellow solution. The TiO_2 nanoparticles were formed by dropwise addition of 62.5 ml of titanium tetra-isopropoxide (TTIP, Acros, 98%) to this solution under vigorous stirring. A part of colloidal solution was dried at 373 K to form a powder, and further annealed at 773 K in air to improve the crystallinity and to ensure that the Fe ions are incorporated as substitutional dopants in the TiO_2 lattice [16]. The remaining colloidal suspensions were tape-casted onto a blank glass substrate (Schott Borofloat 33) to form a thin mesoporous film. Undoped TiO_2 nanopowders were prepared in a similar manner by omitting the $Fe(NO_3)_3$ precursor.

2.2. Catalyst characterization

The crystal structures of the Fe-doped TiO_2 nanoparticles were determined by X-ray diffraction (XRD, Bruker, D8 Advance) with Cu-K_α radiation. UV–vis spectra of the samples were recorded on a Perkin-Elmer Lambda 900 spectrometer with an integrating sphere assembly. A $BaSO_4$ standard was used as a reference sample for baseline correction. Particle morphologies were studied by high resolution transmission electron microscopy (TEM) using a FEI TECNAI TF20 electron microscope equipped with a field emission gun (FEG) and an energy dispersive X-ray (EDX) system for elemental analysis. The sample powders for TEM-EDX measurements were dispersed in an ethanol solution and a few drops of the suspension were placed onto a Quantifoil® carbon polymer-supported copper grid, following by drying at ambient conditions.

The valence state of the Fe dopants was analyzed by X-ray photoelectron spectroscopy (XPS, Thermo Escalab 250) with a monochromatic Al K_α X-ray source. A quartz window on the UHV chamber allowed UV irradiation of the sample surface during the XPS measurement (LC8 spot light source, Hamamatsu). The 1s peak of adventitious carbon at 284.6 eV was used as an internal reference for calibrating the XPS binding energy.

2.3. DRIFTS experiments

In situ diffuse reflectance infrared Fourier transformed spectroscopy (DRIFT, Thermo Nicolet Nexus with a MCT/A detector) was used for monitoring the presence of adsorbed NO, N_2O and NO_2 species on the nanopowder surface. The temperature-controlled chamber was equipped with two CaF_2 windows for the IR measurements, and a quartz window that allowed in situ excitation of the sample. A 150 W Xe lamp with a 370 nm bandpass filter (Newport type 10BPF10-370) served as a UV excitation source. A continuous flow of He (99.999%, O_2 < 5 ppm) with relatively high concentrations of either NO, NO_2 or N_2O (167 ppm, 30 ml/min) was used to ensure efficient adsorption of the target species. Prior to the experiments, the system was checked for leaks with a He leak detector. All DRIFT spectra represent the average of 64 consecutive scans with a resolution of 2 cm^{-1} at 303 K, and are referenced to the sample background.

2.4. Chemoluminescence experiments

The NO_x present in the gas phase during the photocatalytic process is directly detected by an on-line chemiluminescence-based NO_x analyzer (Teledyne Instruments, Model: 200E) with a sensitivity range of 0–2 ppm. The analyzer measures the concentrations of NO and NO_x (=NO + NO_2), and calculates the NO_2 concentration from the difference between these values. A continuous flow of NO/He gas (~1 ppm, 1 l/min) was used as initial target pollutant. The mesoporous thin film samples (10 cm × 5 cm) were placed into a rectangular PMMA reactor (40 cm × 10 cm × 5 cm), in accordance with NEN-ISO 22197-1:2007. A facial tanner (75 W, Philips HB172) was used as a UV light source, providing a UV intensity of 1.76 mW/cm^2 at the sample surface. The intensity of UV light source was measured by a Lutron UVA light meter (model: UVA-365).

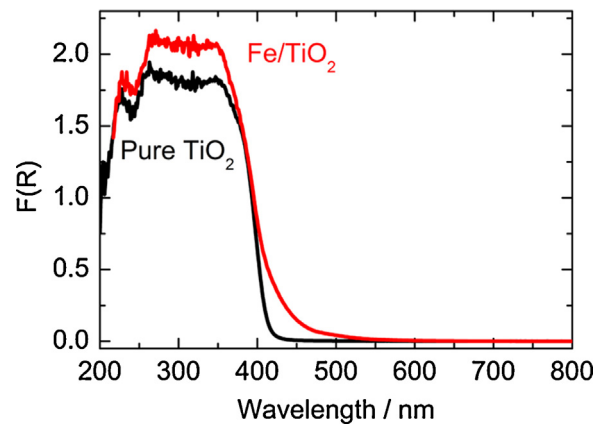

Fig. 1. UV–vis diffuse reflection spectra of pure TiO_2 and 1% Fe/TiO_2 nanoparticles. $F(R)$ is the Kubelka–Munk function, which is defined as $F(R) = (1-R)^2/2R$, with R being the measured reflection ($R = R_{sample}/R_{standard}$) [18].

3. Results and discussion

UV–vis diffuse reflection spectra have been recorded to investigate how the Fe dopant is incorporated into the samples. The results are shown in Fig. 1. The steep increase of the absorption at ~400 nm is due to the indirect band gap of pure anatase TiO_2 [19]. Compared with pure TiO_2, Fe-doped TiO_2 shows a small red shift of the absorption onset toward the visible region. This is attributed to the charge-transfer transition between the *d*-electrons of Fe and the conduction band of the TiO_2 [20], which indicates that Fe is present as a substitutional dopant inside the TiO_2 nanoparticles [17].

The particle morphologies and Fe distribution in the samples are investigated by TEM and EDX measurements, respectively. The TEM image in Fig. 2a reveals a particle size of ~10 nm for 1% Fe-doped TiO_2. Close inspection of a higher resolution TEM image (Fig. 2b) reveals fringes separated by 0.35 nm. This indicates the presence of the anatase form of TiO_2 (d_{101} = 0.35 nm), which is further confirmed by the main anatase (1 0 1) peak in the XRD pattern (Fig. 2c). Compared to pure TiO_2, a small but significant peak shift of the anatase (1 0 1) toward higher 2-theta angles is found for Fe-doped TiO_2, which indicates a small decrease in the (1 0 1) lattice spacing. This is attributed to the formation of oxygen vacancies that charge-compensate the Fe acceptor-type dopants [17]. In addition, a small rutile peak is also found for both pure TiO_2 and Fe-doped TiO_2. The anatase-to-rutile peak intensity ratio decreases with increasing Fe concentration (Fig. 2c), which is in accordance with reports that cation doping favors the anatase-to-rutile phase transformation [21].

In order to determine the Fe distribution in the nanoparticles, the EDX beam was focused at the edge and at the center of a particle, indicated as regions 1 and 2 in Fig. 2b, respectively. The EDX signals from these regions are shown in Fig. 2d. Two obvious Ti peaks (4.49 keV, 4.93 keV) and a small Fe peak at ~6.37 keV are present. Integration of the peak areas indicates nearly the same

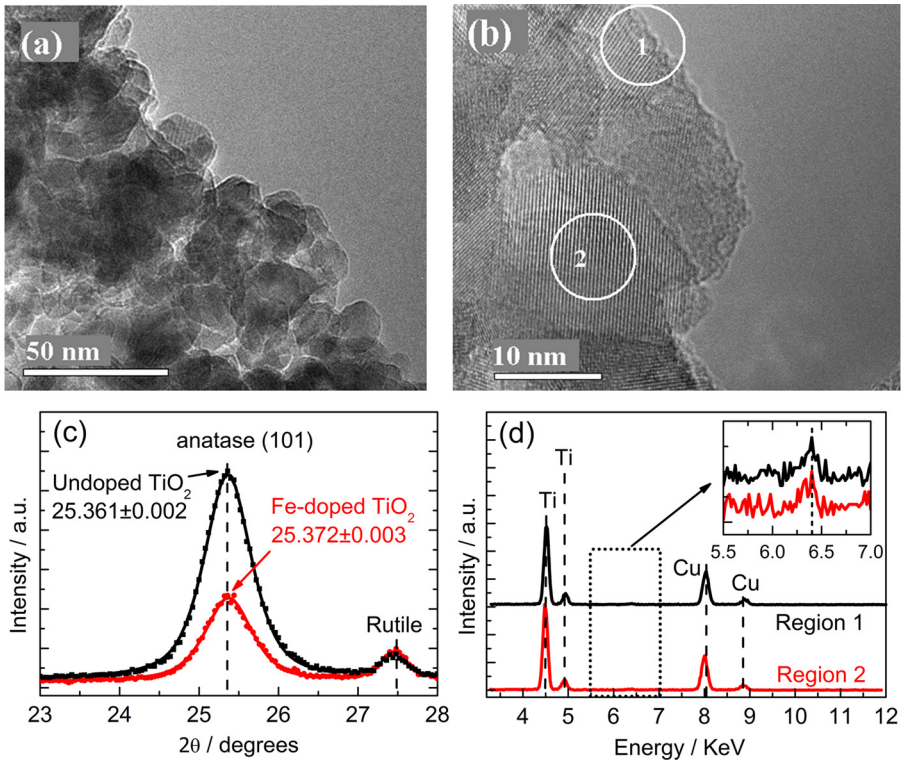

Fig. 2. (a) TEM image of 1% Fe-doped TiO_2; (b) high resolution TEM image of 1% Fe-doped TiO_2; (c) XRD patterns of undoped TiO_2 and 1% Fe-doped TiO_2, fitted with a pseudo-Voigt function; (d) EDX spectra of 1% Fe-doped TiO_2 focused on regions 1 and 2 shown in b). The Cu peaks originate from the support grid.

Fe:Ti ratios for region 1 (0.9 ± 0.3%) and region 2 (1.2 ± 0.4%). This suggests that no significant accumulation of Fe at the surface of the particle occurs.

To gain more insight into the photocatalytic reaction mechanism, DRIFT spectra of undoped TiO_2 and Fe-doped TiO_2 were measured in the presence of NO to investigate the presence of adsorbed intermediates. Before UV irradiation (in the dark), the DRIFT spectrum of undoped TiO_2 in the presence of NO shows a series of clear IR absorption bands (Fig. 3a). These bands are attributed to adsorbed H_2O (1620 cm^{-1}), monodentate nitrate ($-NO_3^-$, 1520 cm^{-1}), monodentate nitrito ($-ONO^-$, 1470 cm^{-1}), nitrite ($-NO_2^-$, 1299 cm^{-1}), and bidentate nitrate (1192 cm^{-1}) groups [4,22,23]. After turning on the UV light, the intensities at 1520 cm^{-1} and 1470 cm^{-1}, and to lesser extent those at 1299 cm^{-1} and 1192 cm^{-1}, show a modest increase. Since all samples were calcined at 500 °C before performing the photocatalytic reactions, it seems unlikely that the IR signals are due to unreacted nitrate groups from the nitric acid or the iron nitrate precursor used during synthesis. An IR spectrum of Fe-doped TiO_2 in He, using KBr as background, indeed did not reveal any nitrate signal. Moreover, XPS measurements on calcined Fe-doped TiO_2 powder (not shown) did not reveal a significant signal at the N-1s binding energy of 398 eV. Based on this, we conclude that the nitric groups in the IR spectra are formed by the photocatalytic oxidation of NO under UV irradiation.

After illumination, the IR spectrum also shows a new small band at 1360 cm^{-1}, which is attributed to adsorbed NO_2 on the anatase surface [24]. This indicates the photocatalytic oxidation of NO to NO_2 in the presence of surface-adsorbed O_2 [25,26] and residual O_2 gas in the He supply (up to 5 ppm). Note that the presence of surface adsorbed O_2 is evidenced by the IR band at 1550 cm^{-1} in Fig. 3b. Once formed, NO_2 quickly desorbs from the TiO_2 surface, and its short residence time explains the relatively small signal of the 1360 cm^{-1} band. The increased intensities of the bands at 1520 cm^{-1} (NO_3^-) and 1360 cm^{-1} (NO_2) upon illumination are consistent with the reaction mechanism that we recently proposed [15]:

$$h\nu \xrightarrow{TiO_2} e^- + h^+ \quad (1)$$

$$Ti(O_2)_{ads} + e^- \xrightarrow{k_1} Ti(O_2^-)_{ads} \quad (2)$$

$$Ti - OH^- + h^+ \rightarrow Ti - OH^\bullet \quad (3)$$

$$Ti(O_2^-)_{ads} + NO(g) \rightarrow Ti(NO_3^-)_{ads} \quad (4)$$

$$Ti - OH^\bullet + NO \rightarrow Ti - H + NO_2(g) \quad (5)$$

Since NO_3^- cannot spontaneously desorb, reactions (2) and (4) will stop after the surface becomes saturated with NO_3^-. However, the band at 1360 cm^{-1} remains present, even after saturation, indicating continued production of NO_2 via reactions (3) and (5). This means that there must be an alternative reaction pathway for the photo-generated electrons. A likely pathway is the reduction of protonated Ti^{4+} sites, resulting in the formation of surface hydroxyls via hydrogenperoxo species [15]:

$$Ti - H + O_2(g) + e^- \xrightarrow{k_2} Ti - OOH^- \quad (6)$$

$$Ti - OOH^- + Ti - H \rightarrow Ti - OH^- + Ti - OH^\bullet \quad (7)$$

$$Ti - OH^\bullet + e^- \rightarrow Ti - OH^- \quad (8)$$

After achieving steady state conditions, reactions (1), (3), (5) and (6)–(8) all occur simultaneously and can be summed up to give:

$$2NO(g) + O_2(g) + 2h\nu \xrightarrow{TiO_2} 2NO_2(g) \quad (9)$$

For Fe-doped TiO_2 under UV irradiation, a small increase of the IR intensities at 1520 cm^{-1}, 1470 cm^{-1}, 1299 cm^{-1}, and a larger increase at 1192 cm^{-1} are observed (Fig. 3b). The ratio at which

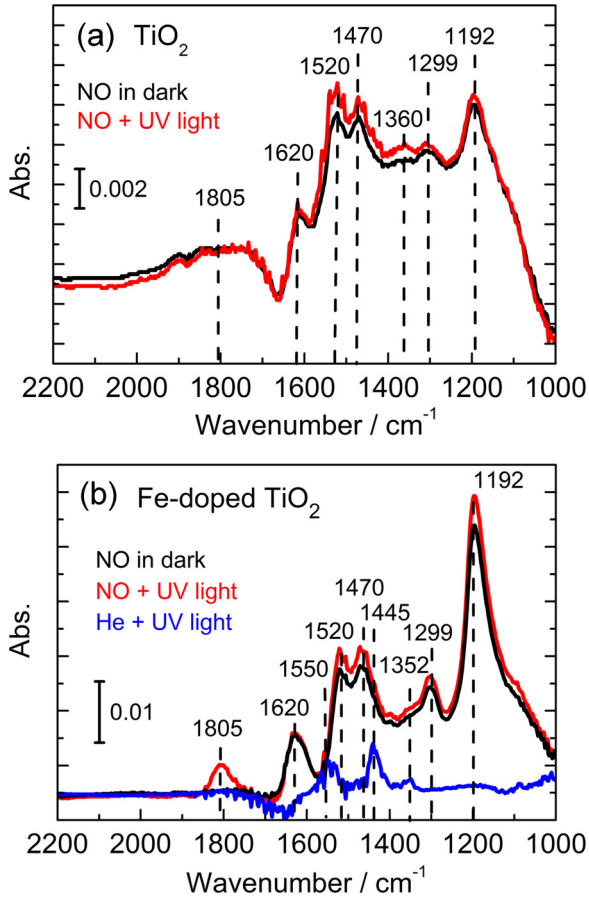

Fig. 3. (a) DRIFT spectra of undoped TiO_2 in the presence of 167 ppm NO in the dark and under UV irradiation; (b) similar spectra and blank test (UV light irradiation in pure He) for 1% Fe-doped TiO_2. The bands at 1352 cm^{-1}, 1445 cm^{-1} and 1550 cm^{-1} in the absence of NO are assigned to adventitious hydrocarbon oxides, bidentate carbonate and adsorbed O_2 [29–31], respectively. (For interpretation of the references to color in the text, the reader is referred to the web version of the article.)

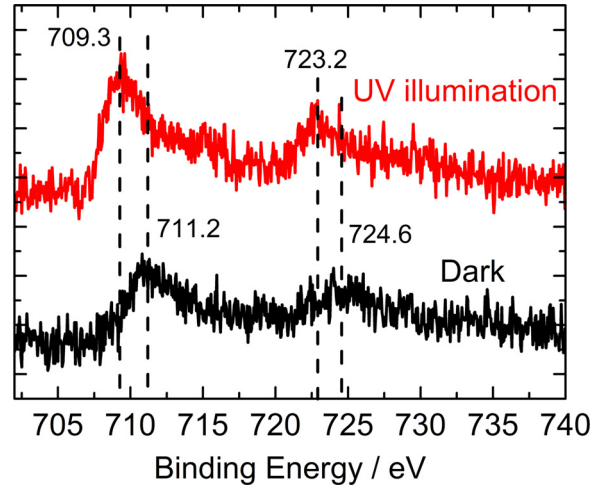

Fig. 4. In situ Fe-2p XPS spectra of 1% Fe-doped TiO_2 in the dark and under UV irradiation.

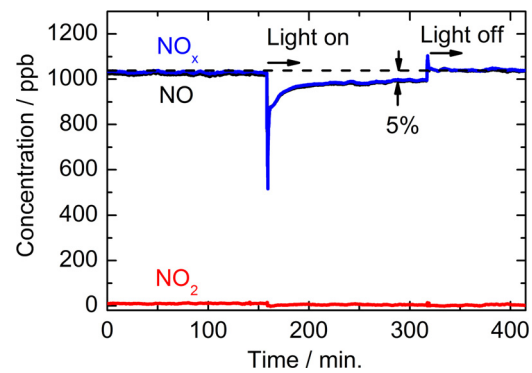

Fig. 5. Photocatalytic degradation of NO over 1% Fe/TiO_2 in pure He atmosphere.

these bands increase suggests that the formation of bidentate nitrate groups (1192 cm^{-1}) is preferred over that of monodentate nitric groups in Fe-doped TiO_2. We attribute this to the larger concentration of oxygen vacancies in the Fe-doped samples [17], which leaves more room at adjacent Ti^{4+} ions for a bidentate coordination. Another difference compared to the spectra for undoped TiO_2 is the absence of the band at 1360 cm^{-1}. This indicates that NO_2 formation is suppressed by Fe doping. A more detailed explanation for this will be given later (vide infra).

The most obvious spectral change for the Fe-doped TiO_2 in Fig. 3b is the appearance of a pronounced band at 1805 cm^{-1} under UV illumination. This band is not present for undoped TiO_2 under the same experimental conditions, nor is it present for Fe/TiO_2 in the absence of NO (Fig. 3b, blue curve). This suggests it is due to a photo-converted NO species adsorbed at a Fe surface site. Although NO-related photocatalytic reaction products for various oxides containing Fe^{2+} and Fe^{3+} ions have been extensively studied by IR spectroscopy [28], the band at 1805 cm^{-1} has not yet been assigned in the literature.

To further investigate the origin of the band at 1805 cm^{-1}, we first clarify the valence state of the Fe ions at the surface of the sample by comparing the XPS spectra in the dark and under UV irradiation. As shown in Fig. 4, the dark spectrum of Fe-doped TiO_2 show peaks at 711.2 eV and 724.6 eV, which correspond to the Fe $2p_{3/2}$ and Fe $2p_{1/2}$ binding energies of Fe^{3+}, respectively [32]. Under UV irradiation the peaks at 711.2 eV and 724.6 eV shift to 709.3 eV and 723.2 eV, respectively, which indicates the presence of Fe^{2+} [33,34]. These results show that most – if not all – of the Fe^{3+} ions are reduced to Fe^{2+} by the photo-generated electrons [35]:

$$Fe^{3+} + e^- \xrightarrow{k_3} Fe^{2+} \quad (10)$$

This reaction only starts after the surface is saturated with NO_3^- species. This is because the electrons first prefer to reduce O_2, since the O_2/O_2^- energy level is positioned slightly below the TiO_2 conduction band minimum [36], while the Fe^{3+}/Fe^{2+} energy level is located slightly above it [37]. After saturation, reactions (2) and (4) can no longer occur, and reduction of Fe^{3+} to Fe^{2+} can take place instead. The consumption of the photo-generated electrons by Fe^{3+} would also inhibit reaction (6) and suppress the formation of NO_2. This explains why the band at 1360 cm^{-1} is not observed for Fe-doped TiO_2 in Fig. 3b.

Direct evidence that the presence of Fe indeed suppresses the formation of NO_2 is shown in Fig. 5. After turning on the UV light, the NO concentration briefly decreases due to the formation of surface nitrates. When the surface is saturated with NO_3^-, the NO concentration at the reactor outlet increases again. As discussed in detail in our previous paper [15], the NO concentration does not go back to its initial value, since ~5% is continuously converted into N_2 and O_2. More importantly, no NO_2 formation occurs, whereas similar experiments for undoped TiO_2 show that 50% of the NO is photo-oxidized to NO_2 [15].

The Fe^{2+} that is formed is a well known and efficient adsorption site for NO [38]. Therefore, the band at 1805 cm^{-1} in Fig. 3b may be due to an NO reaction product coordinated to Fe^{2+}. Possible NO

Table 1
Observed N—O stretching modes of NO_x species coordinated to various Fe surface sites.

Wavenumber (cm^{-1})	Assignment	Catalyst	Reference
2250	$Fe^{2+}(N_2O)$	Fe-ZSM-5	[41]
1824	$Fe^{2+}(NO)$	$FeAl_2O_4$	[42]
1845–53	$Fe^{2+}(NO)$	$FeTiO_3$	[42]
1810	$Fe^{2+}(NO)_2$	Fe/SiO_2	[37]
1805	$Fe^{2+}(NO)_2$	Fe-doped TiO_2	This paper
1840	$Fe^{3+}(NO)$	Fe-doped TiO_2	[16]
1625	$Fe^{2+}(NO_2)$	Fe-ZSM-5	[43]
1575	$Fe^{n+}(NO_3)$	Fe-ZSM-5	[43]
1914, 1900	$Ti^{4+}(NO)_n$	TiO_2	[44]
1798–1811	$Fe^{2+}(NO)_2$	Molecular species	[45]

reaction products, other than the nitrate, nitrito and nitrite species identified above, are neutral nitrosyl (NO), NO_2 and N_2O species. To investigate these possibilities, DRIFT spectra were recorded with gaseous NO_2 and N_2O as the target species, in the dark and under UV illumination. No peak at 1805 cm^{-1} was observed for any of these measurements, which shows that the IR band at 1805 cm^{-1} cannot be attributed to adsorbed NO_2 or N_2O.

This leaves the possibility that the band at 1805 cm^{-1} is due to a nitrosyl species. The vibrational frequency indeed falls within the range of 1966–1710 cm^{-1} that is associated with various forms of adsorbed NO [23]. For ternary Fe-containing oxides, Miyata et al. reported $Fe^{2+}(NO)$ bands in the range of 1826–1853 cm^{-1} (Table 1). A somewhat lower frequency of 1810 cm^{-1} was found for the $Fe^{2+}(NO)_2$ di-nitrosyl species in Fe/SiO_2 [39]. Comparable values of 1798 and 1811 cm^{-1} were reported for molecular $Fe(NO)_2$ species condensed in either argon or neon gases, respectively [45]. In the solid state, the coordination of two nitrosyl species to a single Fe^{2+} ion would require slightly more free space around this ion. In our case, this space can be provided by the presence of oxygen vacancies that charge-compensate the Fe dopant. Taking all these considerations into account, we assign the band at 1805 cm^{-1} to a dinitrosyl species coordinated to Fe^{2+} sites in Fe-doped TiO_2. The formation of this species can be described by reactions (1), (10) and (11):

$$Fe^{2+} + 2NO \rightarrow Fe^{2+}(NO)_{2,ads} \quad (11)$$

It should be noted that the frequency of the N=O stretch vibration in $Fe^{2+}(NO)_2$ is significantly lower than that of gaseous NO (1876 cm^{-1}) [40]. This is due to back-donation of the Fe^{2+} *d*-electrons to the π^* antibonding orbitals of the NO molecules [13]. This back-donation weakens the N—O bond, resulting in a lower vibration frequency. Another consequence of back-donation is that it stabilizes the interaction between Fe^{2+} and NO, which explains why dinitrosyls are commonly observed on transition metal ions rich in *d*-electrons [46].

To better understand the nature of the adsorbed dinitrosyl species, a series of DRIFT spectra are recorded immediately after turning off the UV light. As shown in Fig. 6, the band at 1805 cm^{-1} rapidly decreases within the first 5 min and has completely disappeared after 40 min, while other nitric bands (e.g. 1520 cm^{-1}, 1470 cm^{-1}, 1299 cm^{-1} and 1192 cm^{-1}) remain the same. This shows that the NO species adsorbed at the Fe^{2+} sites ($Fe^{2+}(NO)_{2,ads}$) spontaneously desorb. This is attributed to the re-oxidation of Fe^{2+} to Fe^{3+} by an adjacent hydroxyl radical that was previously formed through reaction (3) [15]:

$$Fe^{2+}(NO)_2 + Ti-OH^{\bullet} \rightarrow Fe^{3+}(NO)_{2,ads} + Ti-OH^{-} \quad (12)$$

The re-oxidation of Fe^{2+} to Fe^{3+} reduces the amount of π back bonding [16]. This decreases the stability of Fe—NO bond and explains why NO spontaneously desorbs after turning off the UV light:

$$Fe^{3+}(NO)_{2,ads} \rightarrow Fe^{3+} + 2NO(g) \quad (13)$$

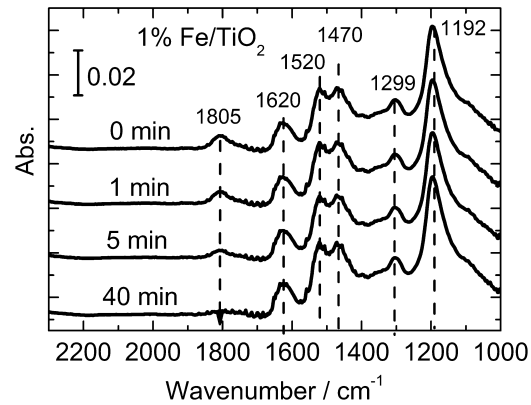

Fig. 6. DRIFT spectra of 1% Fe-doped TiO_2 in a 167 ppm NO/He atmosphere. The band at 1805 cm^{-1} completely disappears within a few minutes after turning off the UV light.

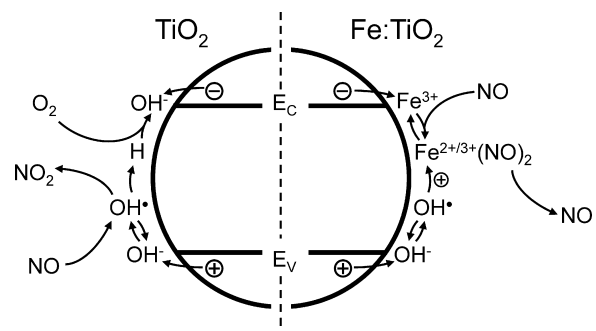

Fig. 7. Suppression of NO_2 formation at the surface of Fe-doped TiO_2 nanoparticles.

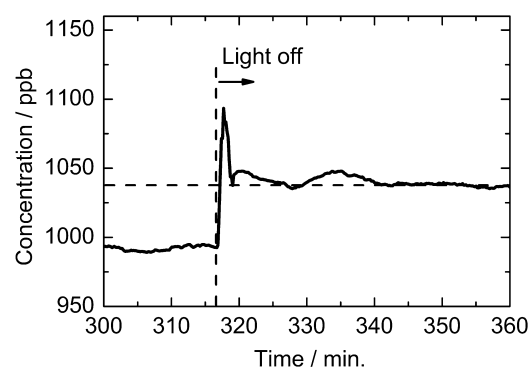

Fig. 8. NO release for 1% Fe-doped TiO_2 after the UV irradiation is turned off.

The sum of reactions (1), (3), and (10)–(13) represents an Fe-mediated recombination mechanism for the photo-generated electrons and holes, which explains why so little NO_2 is formed at the surface of Fe-doped TiO_2 nanoparticles. The difference between the reaction mechanisms for undoped and Fe-doped TiO_2 is illustrated in Fig. 7.

Direct evidence for NO desorption is provided by the on-line NO_x analysis (Fig. 5), at the point where the UV illumination is turned off. An expanded view of this part is shown in Fig. 8. After turning off the UV light, a small amount of released NO is detected by the NO_x analyzer, as evidenced by the peak at $t = 317$ min. Integration of this peak shows that the number of desorbed NO molecules corresponds to ~2% of the total number of Fe sites at the surface.[1]

[1] The total number of desorbed NO molecules was calculated by integrating NO_x curve (from $t = 317.2$ min. to $t = 340.7$ min.) in Fig. 8. The final concentration of

We tentatively attribute this rather small value to the presence of trace amounts of water. We previously showed that H_2O binds more strongly to surface Fe species than NO, so it may block a large part of the available Fe surface sites [16]. An alternative explanation might be that only a small fraction of the surface Fe sites is active, for example those on a step site, where they would experience less steric hindrance.

4. Conclusions

In conclusion, the presence of an Fe dopant in TiO_2 nanoparticles provides a recombination pathway for the photo-generated electrons and holes that suppresses the formation of NO_2 during the photocatalytic decomposition of nitric oxide. XPS evidence shows that Fe^{3+} is photo-reduced to Fe^{2+} under UV illumination. The formation of Fe^{2+} is accompanied by a new IR band at 1805 cm^{-1}, which is assigned to the N=O stretch vibration in a $Fe^{2+}(NO)_2$ complex. This Fe^{2+} is re-oxidized to Fe^{3+} by the photo-generated holes via an adjacent hydroxyl radical group (Ti—OH•), which triggers the release of the NO species. This work demonstrates that dopants can be used to suppress undesired reactions at metal oxide surfaces, offering a convenient and effective way to develop highly selective photocatalysts.

Acknowledgements

The authors gratefully acknowledge the kind help from B. van der Linden of the Catalysis Engineering group at Delft University of Technology and G. Mul from the University of Twente with the DRIFTS experiments. Financial support for this work is provided by the Shell-TU Delft "Sustainable Mobility" program.

References

[1] J.A. Rodriguez, T. Jirsak, G. Liu, J. Hrbek, J. Dvorak, A. Maiti, Journal of the American Chemical Society 123 (2001) 9597–9605.
[2] S. Devahasdin, C. Fan, K. Li, D.H. Chen, Journal of Photochemistry and Photobiology A 156 (2003) 161–170.
[3] M. Kitano, M. Matsuoka, M. Ueshima, M. Anpo, Applied Catalysis A 325 (2007) 1–14.
[4] J.C.S. Wu, Y.T. Cheng, Journal of Catalysis 237 (2006) 393–404.
[5] W. Shan, F. Liu, H. He, X. Shi, C. Zhang, Chemical Communications 47 (2011) 8046–8048.
[6] (a) Y. Ohko, Y. Nakamura, N. Negishi, S. Matsuzawa, K. Takeuchi, Journal of Photochemistry and Photobiology A 205 (2009) 28–33;
(b) H. Chen, C.E. Nanayakkara, V.H. Grassian, Chemical Reviews 112 (2012) 5919–5948;
(c) R.V. Mikhaylov, A.A. Lisachenko, B.N. Shelimov, V.B. Kazansky, G. Martra, G. Alberto, S. Coluccia, The Journal of Physical Chemistry C 113 (2009) 20381–20387.
[7] Z. Zhang, C.C. Wang, R. Zakaria, J.Y. Ying, Journal of Physical Chemistry B 102 (1998) 10871–10878.
[8] X.H. Wang, J.-G. Li, H. Kamiyama, M. Katada, N. Ohashi, Y. Moriyoshi, T. Ishigaki, Journal of the American Chemical Society 127 (2005) 10982–10990.
[9] J.M. Coronado, A.J. Maira, J.C. Conesa, K.L. Yeung, V. Augugliaro, J. Soria, Langmuir 17 (2001) 5368–5374.
[10] M.R. Hoffmann, S.T. Martin, W. Choi, D.W. Bahnemann, Chemical Reviews 95 (1995) 69–96.
[11] T.H. Lim, S.M. Jeong, S.D. Kim, J. Gyenis, Journal of Photochemistry and Photobiology A 134 (2000) 209–217.
[12] S. Laufs, G. Burgeth, W. Duttlinger, R. Kurtenbach, M. Maban, C. Thomas, P. Wiesen, J. Kleffmann, Atmospheric Environment 44 (2010) 2341–2349.
[13] J. Zhang, Y. Hu, M. Matsuoka, H. Yamashita, M. Minagawa, H. Hidaka, M. Anpo, Journal of Physical Chemistry B 105 (2001) 8395–8398.
[14] J. Yang, C. Chen, H. Ji, W. Ma, J. Zhao, Journal of Physical Chemistry B 109 (2005) 21900–21907.
[15] Q. Wu, R. van de Krol, Journal of the American Chemical Society 134 (2012) 9369–9375.
[16] Q. Wu, G. Mul, R. van de Krol, Energy & Environmental Science 4 (2011) 2140–2144.
[17] Q. Wu, Q. Zheng, R. van de Krol, Journal of Physical Chemistry C 116 (2012) 7219–7226.
[18] C. Anderson, A.J. Bard, Journal of Physical Chemistry B 101 (1997) 2611–2616.
[19] X. Li, P. Yue, C. Kutal, New Journal of Chemistry 27 (2003) 1264–1269.
[20] J. Zhu, F. Chen, J. Zhang, H. Chen, M. Anpo, Journal of Photochemistry and Photobiology A 180 (2006) 196–204.
[21] C.S. Enache, J. Schoonman, R. van de Krol, Applied Surface Science 252 (2006) 6342–6347.
[22] K. Hadjiivanov, H. Knözinger, Physical Chemistry Chemical Physics 2 (2000) 2803–2806.
[23] K. Hadjiivanov, V. Bushev, M. Kantcheva, D. Klissurski, Langmuir 10 (1994) 464–471.
[24] T.J. Dines, C.H. Rochester, A.M. Ward, Journal of the Chemical Society – Faraday Transactions 87 (1991) 643–651.
[25] J.C. Yu, J. Lin, D. Lo, S.K. Lam, Langmuir 16 (2000) 7304–7308.
[26] J.S. Dalton, P.A. Janes, N.G. Jones, J.A. Nicholson, K.R. Hallam, G.C. Allen, Environmental Pollution 120 (2002) 415–422.
[28] M. Rivallan, G. Ricchiardi, S. Bordiga, A. Zecchina, Journal of Catalysis 264 (2009) 104–116.
[29] S.S. Malwadkar, R.S. Gholap, S.V. Awate, P.V. Korake, M.G. Chaskar, N.M. Gupta, Journal of Photochemistry and Photobiology A 203 (2009) 24–31.
[30] I.X. Green, J.T. Yates, Journal of Physical Chemistry C 114 (2010) 11924–11930.
[31] W. Su, J. Zhang, Z. Feng, T. Chen, P. Ying, C. Li, Journal of Physical Chemistry C 112 (2008) 7710–7716.
[32] Y. Zhang, Y. Shen, F. Gu, M. Wu, Y. Xie, J. Zhang, Applied Surface Science 256 (2009) 85–89.
[33] J. Arana, O.G. Díaz, J.M.D. Rodríguez, J.A.H. Melián, C.G. Cabo, J.P. Pena, M.C. Hidalgo, J.A. Navío-Santos, Journal of Molecular Catalysis A 197 (2003) 157–171.
[34] M. Descostes, F. Mercier, N. Thromat, C. Beaucaire, M. Gautier-Soyer, Applied Surface Science 165 (2000) 288–302.
[35] W. Hung, Y. Chen, H. Chu, T. Tseng, Applied Surface Science 255 (2008) 2205–2213.
[36] A. Fujishima, T.N. Rao, D.A. Tryk, Journal of Photochemistry and Photobiology C 1 (2000) 1–21.
[37] W. Choi, A. Termin, M.R. Hoffmann, Journal of Physical Chemistry 98 (1994) 13669–13679.
[38] G. Mul, J. Pérez-Ramírez, F. Kapteijn, J.A. Moulijn, Catalysis Letters 80 (2002) 129–138.
[39] S. Yuen, Y. Chen, J.E. Kubsh, J.A. Dumesic, N. Topsoe, H. Topsoe, Journal of Physical Chemistry 86 (1982) 3022–3032.
[40] K.P. Huber, G. Herzberg, Molecular Spectra and Molecular Structure, vol. 4, Van Nostrand, Princeton, NJ, 1979.
[41] A. Wacław, K. Nowińska, W. Schwieger, A. Zielińska, Catalysis Today 90 (2004) 21–25.
[42] H. Miyata, Y. Nakagawa, S. Miyagawa, Y. Kubokawa, Journal of the Chemical Society – Faraday Transactions 84 (1998) 2129–2134.
[43] G.D. Pirngruber, J.A.Z. Pieterse, Journal of Catalysis 237 (2006) 237–247.
[44] G. Ramis, G. Busca, V. Lorenzelli, Applied Catalysis 64 (1990) 243–257.
[45] M. Zhou, L. Andrews, Journal of Physical Chemistry A 104 (2000) 3915–3925.
[46] K.I. Hadjiivanov, Catalysis Reviews – Science & Engineering 42 (2000) 71–144.

1040 ppb was used as a baseline. With 0.019 g of thin film sample, a BET surface area of 71 m^2/g, and a Fe:Ti ratio of 1%, this corresponds to ~2% of the total number of Fe surface sites.